Interference with ENO2 promotes ferroptosis and inhibits glycolysis in clear cell renal cell carcinoma by regulating Hippo-YAP1 signaling

HU LI[1], YANNI WU[2], YONG MA[3] and XIAOQIANG LIU[1]

[1]Department of Urology, Tianjin Medical University General Hospital, Tianjin 300052; [2]Department of Medical Technology, Heze Jiazheng Vocational College; [3]Department of Urology, Shanxian Central Hospital, Affiliated Huxi Hospital of Jining Medical University, Heze, Shandong 274300, P.R. China

Received November 2, 2023; Accepted February 12, 2024

DOI: 10.3892/ol.2024.14576

Abstract. Glycolytic enzyme enolase 2 (ENO2) is dysregulated in various cancer types. Nevertheless, the role and underlying mechanism of ENO2 in clear cell renal cell carcinoma (ccRCC) remain unclear. Therefore, the current study investigated the effect and mechanism of ENO2 in ccRCC. ENO2 expression in a ccRCC cell line was assessed using reverse transcription-quantitative PCR and western blotting. Analysis of glycolysis was performed by estimating the extracellular acidification rate, lactic acid concentration, glucose uptake and the expression of glucose transporter 1, pyruvate kinase muscle isozyme M2 and hexokinase 2. Moreover, ferroptosis was assessed by detecting the level of total iron, lipid peroxide, reactive oxygen species and the expression of ferroptosis-related protein. In addition, mitochondrial function was assessed using JC-1 staining and detection kits. The results indicated that ENO2 is expressed at high levels in ccRCC cell lines, and interference with ENO2 expression inhibits glycolysis, promotes ferroptosis and affects mitochondrial function in ccRCC cells. Further investigation demonstrated that interference with ENO2 expression affected ferroptosis levels in ccRCC cells by inhibiting the glycolysis process. Mechanistically, the present results indicated that ENO2 may affect ferroptosis, glycolysis and mitochondrial functions by regulating Hippo-yes-associated protein 1 (YAP1) signaling in ccRCC cells. In conclusion, the present study showed that ENO2 affects ferroptosis, glycolysis and mitochondrial functions in ccRCC cells by regulating Hippo-YAP1 signaling, hence demonstrating its potential as a therapeutic target in ccRCC.

Correspondence to: Dr Xiaoqiang Liu, Department of Urology, Tianjin Medical University General Hospital, 154 Anshan Road, Heping, Tianjin 300052, P.R. China
E-mail: drliuxq2023@163.com

Key words: enolase 2, clear cell renal cell carcinoma, glycolysis, ferroptosis, mitochondrial function, Hippo-YAP1 signaling

Introduction

Papillary renal cell carcinoma (PRCC) affects >400,000 people worldwide each year, mainly affecting people >60 years old, with 2/3 of patients being male (1). Among them, clear cell (cc) RCC is the most prevalent type of kidney cancer, an aggressive cancer that originates from the proximal tubular epithelium and its metastatic form is closely associated with high mortality (2). Although early detection allows ccRCC to be successfully treated with surgical or ablation strategies, ≤1/3 of patients have or develop metastases (3). Metastatic ccRCC is almost always fatal and is biologically different from non-metastatic disease; therefore, exploring its underlying mechanisms is crucial to developing anti-ccRCC therapeutic options.

Cancer cells sustain a unique energy metabolism network to facilitate cell survival, growth, progression and metastasis in adverse environments (4). Glycolysis is the initial process in the breakdown of glucose to harness energy for cellular metabolism. During glycolysis, cancer cells take up more glucose than healthy cells, and lactic acid is produced from pyruvate which reduces the pH of the tumor (5). A recent study confirmed that glycolysis is closely related to invasion status, clinical stage, patient prognosis and tumor drug resistance, and affects the occurrence and development of ccRCC (6). Moreover, ferroptosis is a form of non-apoptotic cell death driven by iron-dependent lipid peroxidation, which is associated with a variety of metabolic disorders and disruption of homeostasis. In addition, ferroptosis has been studied in hepatocellular carcinoma, and breast, lung, pancreatic, gastric and cervical cancer, and other tumors exhibiting ferroptosis suppression (7). Furthermore, ferroptosis is associated with numerous physiological processes such as mitochondrial function, lipid metabolism and oxidative stress; induction of ferroptosis plays a pivotal role in inhibiting tumor progression (8). The core mechanism of ferroptosis is lipid peroxidation which is dependent on iron and its impact on tumors still exists in ccRCC (9,10).

Enolase 2 (ENO2), a crucial member of the enolase family, is the rate-limiting enzyme in glycolysis catalyzing the conversion of 2-phosphoglycerate to phosphoenolpyruvate (11,12). ENO2,

which mainly exists in neuroendocrine tissues and neurons, is a long-chain acidic dimer protein with 433 amino acids that encompasses two enolate isoenzymes αγ and γγ (13). ENO2 is a well-established tumor biomarker in various cancers, such as prostate cancer, pancreatic ductal adenocarcinoma, small-cell lung cancer, metastatic neuroblastoma and the microvascular invasion status of liver cancer (12,14). Recent studies demonstrated that overexpression of ENO2 is associated with increased cell proliferation and glycolysis enrichment in PRCC (15-17). A similar trend was also observed in bone marrow mononuclear cells of hematological tumors (18). In addition, ENO2 promotes colorectal cancer metastasis by activating yes-associated protein 1 (YAP1)-induced epithelial-mesenchymal transition, while inhibiting the activation of the Hippo-YAP1 pathway induces ferroptosis in small-cell lung cancer cells (19,20). Tumorigenesis and metastasis of ccRCC can be promoted by regulating microRNA-498/Hippo-YAP1 axis (21). However, to the best of our knowledge, the role of ENO2 in ccRCC has not been extensively studied mechanistically.

The present study aimed to evaluate the effect of ENO2 on ccRCC by regulating the expression of ENO2 and analyzing the mechanism of ENO2 on ccRCC through YAP1 signaling.

Materials and methods

Cell culture and transfection. The HK-2 normal human renal tubular epithelial cell line, and the 786-O, ACHN, Caki-1 and 769-PRCC cell lines were purchased from the American Type Culture Collection. All the cells were cultured in RPMI-1640 (Gibco; Thermo Fisher Scientific, Inc.) supplemented with 10% fetal bovine serum (Biochrom, Ltd.), 100 mg/ml streptomycin and 100 μl/ml penicillin in a humidified atmosphere with 5% CO_2 at 37˚C to adjust the cell concentration to $2x10^6$ cells/ml.

ENO2 small-interfering (si)RNAs, namely si-ENO2#1 and si-ENO2#2, were synthesized by Shanghai GenePharma Co., Ltd., and the corresponding negative control (si-NC) was also obtained. The YAP-overexpressing plasmid DNA (OV-YAP) used to overexpress the YAP gene in cells, and an empty vector control, were obtained from Addgene, Inc. Cells were seeded in 6-well plates for western blotting and cultured for 24 h before treatment. Caki-1 cells were transfected with 100 nM recombinants at 37˚C for 48 h using 6 μl of Lipofectamine® 2000 (Thermo Fisher Scientific, Inc.) and 2 μg of the vector. Reverse transcription-quantitative (RT-q)PCR and western blotting were used to screen the Caki-1 cells transfected with si-ENO2#1 and OV-YAP1 after incubation for 48 h at 37˚C. Transfected cells were then used for subsequent experiments. The sequences of the siRNAs used were as follows: si-ENO2#1, 5'-CCCACAGTGGAGGTGGATCTCTATA-3'; si-ENO2#2, 5'-GGTGGATCTCTATACTGCCAAAGGT-3'; si-NC, 5'-CACTGAAGGTGGAGGTCTTCACATC-3'.

RT-qPCR. Total RNA was extracted using TRIzol® reagent (Invitrogen; Thermo Fisher Scientific, Inc.), and 2 μg first-strand cDNA was synthesized using the Maxima First-Strand Complementary DNA Synthesis Kit (Thermo Fisher Scientific, Inc.) according to the manufacturer's instructions. Maxima SYBR Green qPCR Master Mix (Thermo Fisher Scientific, Inc.) was used to perform qPCR with β-actin was used as the internal reference. The thermocycling conditions were as follows: Initial denaturation at 95˚C for 7 min, followed by 40 cycles of 95˚C for 15 sec and 60˚C for 30 sec, and then a final extension at 72˚C for 30 sec. The $2^{-\Delta\Delta Cq}$ method was used to calculate the relative expression of mRNA. The following primer sets were used for qPCR: ENO2 forward (F), 5'-GTGTCTCTGGCCGTGTGTAA-3', reverse (R), 5'-TCTCCAGGATATTGGGGGCA-3'; GAPDH F, 5'-AATGGGCAGCCGTTAGGAAA-3', R, 5'-GCGCCC AATACGACCAAATC-3'.

Western blotting. Total protein was extracted from cells using RIPA lysis buffer (Beyotime Institute of Biotechnology), and protein content was quantified using a BCA kit (Beyotime Institute of Biotechnology). After protein samples (30 μg/lane) were subjected to protein separation using 10% SDS-PAGE, the bands were transferred onto a PVDF membrane. PVDF membranes were blocked with 5% skim milk at room temperature for 2 h. Membranes were then incubated with primary antibodies against ENO2 (cat. no. A12341; 1:2,000; ABclonal Biotech Co., Ltd.), glucose transporter 1 (cat. no. ab115730; GLUT1; 1:2,000; Abcam), pyruvate kinase muscle isozyme M2 (cat. no. ab85555; PKM2; 1:2,000; Abcam), hexokinase 2 (cat. no. ab209847; HK2; 1:1,000; Abcam), acyl-CoA synthetase long-chain family member 4 (cat. no. PA5-27137; ACSL4; 1:1,000; Thermo Fisher Scientific, Inc.), GSH peroxidase 4 (cat. no. ab125066; GPX4; 1:1,000; Abcam), ferritin heavy chain 1 (cat. no. 3998S; FTH1; 1:1,000; Cell Signaling Technology, Inc.), solute carrier family 7 member 11 (PA1-16893; SLC7A11; 1:1,000; Thermo Fisher Scientific, Inc.), large tumor suppressor kinase 1 (cat. no. PA5-78278; LATS1; 1:1,000; Thermo Fisher Scientific, Inc.), YAP1 (cat. no. ab52771; 1:1,000; Abcam) and GAPDH (cat. no. ab9485; 1:3,000; Abcam) for 12 h at 4˚C. The strips were then incubated with the Goat Anti-Rabbit IgG H&L (HRP-conjugated) secondary antibody (cat. no. ab205718; 1:3,000; Abcam) for 2 h at room temperature, and the signal was detected using an enhanced chemiluminescence kit (Thermo Fisher Scientific, Inc.). Finally, the expression levels were semi-quantitatively analyzed using Image-Pro Plus (version 6.0; Media Cybernetics, Inc.).

Measurement of extracellular acidification rate (ECAR). ECAR was evaluated using the Seahorse XFe 96 Extracellular Flux Analyzer (Seahorse Bioscience; Agilent Technologies, Inc.) with Seahorse XF Glycolysis Stress Test Kit following the manufacturer's protocols. Treated Caki-1 cells were evenly spread on a 24-well XF cell culture plate at a density of $5x10^4$ cells per well. Data of ECAR were assessed using the Seahorse XF-96 Wave software version 2.6 and ECAR is shown in mpH/min.

Ferroptosis analysis. Ferroptosis analysis was carried out using the Iron Assay Kit (ScienCell Research Laboratories, Inc.) in a 96-well plate following the manufacturer's recommendations. To prepare iron standards, cell lysates were homogenized and diluted to ensure absorbance readings fell within the standard curve range. Finally, cell absorbance was measured at 590 nm. PKM2 activator DASA-58 (HY-19330) was purchased from MedChemExpress. DASA-58 (30 μM) was dissolved in dimethyl sulfoxide for 2 days at room temperature and was used for activating PKM2.

The reactive oxygen species (ROS) levels of the cells were evaluated using the ROS Assay Kit (Beyotime Institute of

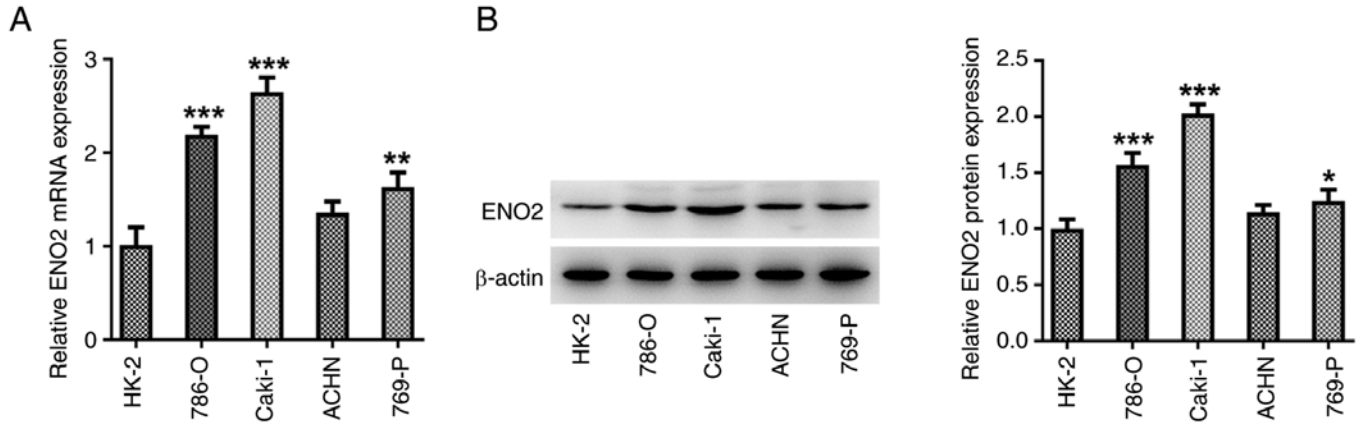

Figure 1. Expression of ENO2 in ccRCC cell lines. (A) Relative ENO2 mRNA expression in ccRCC cell lines. (B) Relative ENO2 protein expression in ccRCC cell lines. *P<0.05, **P<0.01 and ***P<0.001 vs. si-NC. Statistical significance was determined using one-way ANOVA followed by Tukey's post hoc test. ENO2, enolase 2; si-NC, small-interfering RNA negative control; ccRCC, clear cell renal cell carcinoma.

Biotechnology). Briefly, cells were collected and incubated with 100 μM diacetyl dichlorofluorescein (DCFH-DA) for 30 min. Images were captured using a fluorescence microscope (Bx51; Olympus Corporation). Determination of mean fluorescence intensity of dihydroethidium was determined using a FACSCalibur (BD Biosciences). The density of relative fluorescence intensity was analyzed using ImageJ 1.43b software (National Institutes of Health).

Mitochondrial membrane potential assay. Mitochondrial membrane potential was evaluated using JC-1 according to the manufacturer's protocol (Beyotime Institute of Biotechnology). Briefly, Caki-1 cells were cultured in 6-well plates with 3x10^5 cells/well. After 24 h, cells were treated with SPIO-Serum at a concentration of 100 μg Fe/ml for 24 h. Cells were stained with JC-1 for 20 min in the dark at 37˚C and analyzed using flow cytometry as aforementioned (BD Biosciences), and observed under a fluorescence microscope (magnification, x200; Olympus Corporation). The JC-1 excitation wavelength was 488 nm and the approximate emission wavelengths of the JC-1 monomeric and aggregate forms were 529 and 590 nm, respectively.

Detection of biochemical factors. The level of glutathione (GSH) in cell lysates was measured using the GSH Assay Kit (cat. no. CS0260; Sigma Aldrich; Merck KGaA) according to the manufacturer's instructions. The levels of malonaldehyde (MDA) and 4-hydroxynonenal (4-HNE), and the activities of superoxide dismutase (SOD) and GSH-peroxidase (GSH-Px) were determined using commercial MDA, 4-HNE, SOD and GSH-Px assay kits (Nanjing Jiancheng Bioengineering Institute), respectively, following the manufacturer's instructions. Absorbance at 450 nm was recorded, and the data were used to calculate the levels of various cytokines based on the standard curves.

Glucose uptake and lactic acid concentration. Glucose uptake level in ccRCC cells was measured using the Glucose Uptake Assay Kit (colorimetric; cat. no. ab136955; Abcam). To measure lactic acid concentration in culture medium from Caki-1 cells, a lactic acid assay kit (Nanjing Jiancheng Bioengineering Institute) was used according to the manufacturer's instructions. This kit provided a reliable method to assess lactic acid levels, ensuring that the results were consistent and reliable.

Intracellular ATP detection assay. Cells were trypsinized and lysed on ice with lysis buffer provided with an ATP Assay Kit (cat. no. BC0300; Beijing Solarbio Science & Technology Co., Ltd.). The supernatant was then collected and incubated with ATP detection reagent following the manufacturer's instructions. Luminescence was measured using a spectrophotometer (Biotek Synergy H1; BioTek; Agilent Technologies, Inc.) and normalized to the protein concentration.

Mitochondrial function evaluation. Mitochondrial respiration experiment was used to detect mitochondrial oxidative phosphorylation ability. The mitochondrial permeability transition pore (mPTP) assay kit (cat. no. C2009S; Beyotime Institute of Biotechnology) was used to detect the opening of mPTP. Then, Caki-1 cells were seeded into 24-well plates, and 500 μl fluorescence quenching solution was added to each well and incubated for 30 min. The incubating solution was then replaced with preheated DMEM/F12 and incubated in the dark for 30 min. After washing twice with PBS, the cell fluorescence was observed under a fluorescence microscope.

Statistical analysis. All data are expressed as the mean ± standard deviation. The results were analyzed with GraphPad Prism (version 8.0; Dotmatics). One-way ANOVA followed by Tukey's post hoc test was used to compare differences between multiple groups. P<0.05 was considered to indicate a statistically significant difference.

Results

ENO2 is expressed at high levels in ccRCC cell lines. The expression of ENO2 in the ccRCC cell lines 786-O, ACHN, 769-P and Caki-1 was measured using RT-qPCR and western blotting. The expression of ENO2 was significantly higher in ccRCC cell lines compared with that in the HK-2 normal human renal tubular epithelial cell line, with the most pronounced increase in the Caki-1 cells (Fig. 1A and B). Therefore, Caki-1 cells were selected for subsequent experimentation.

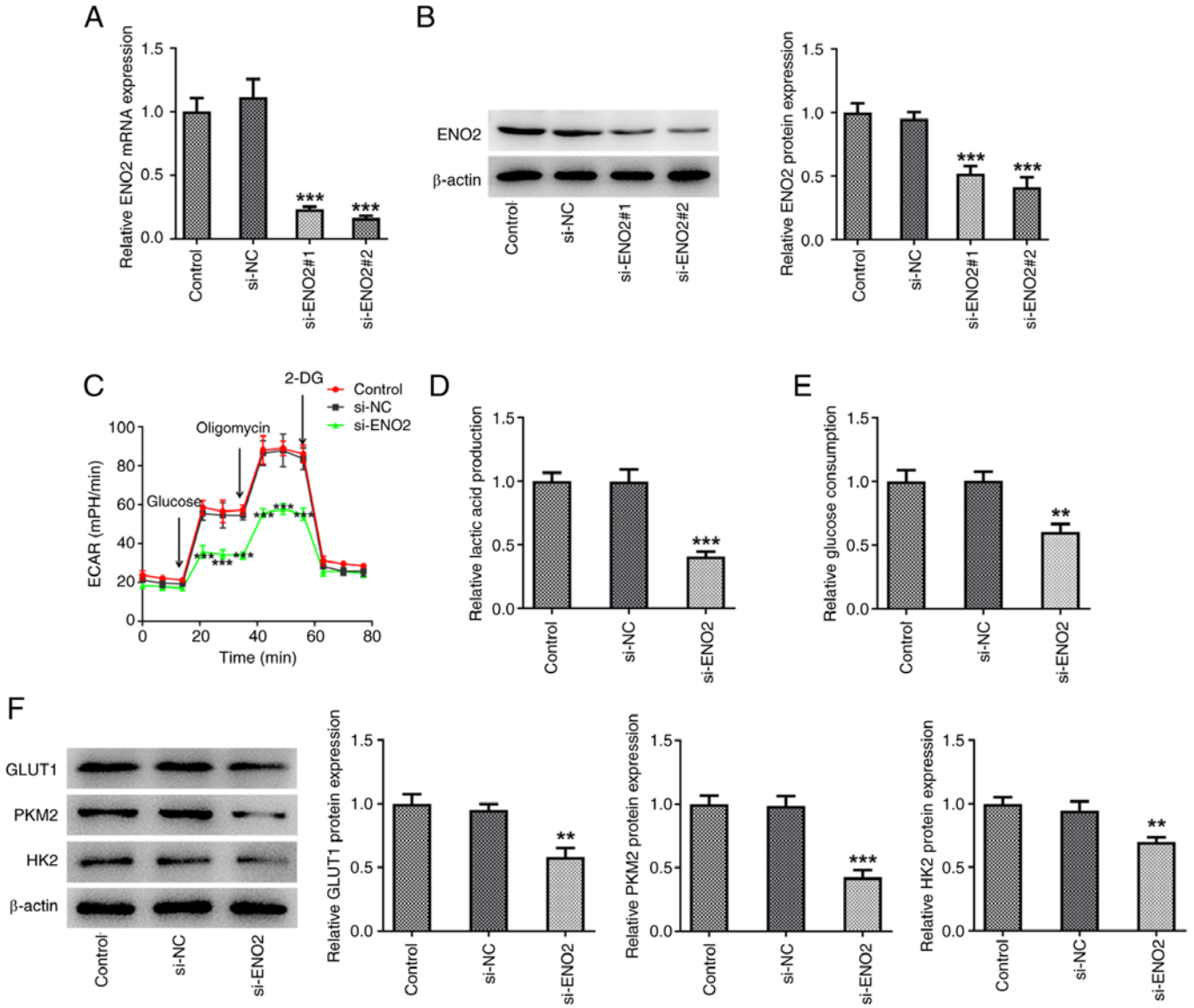

Figure 2. Effects of ENO2 interference on glycolysis in ccRCC cells. (A) Relative ENO2 mRNA expression after interference. (B) Relative ENO2 protein expression after interference. (C) ECAR assessment. (D) Levels of lactic acid. (E) Levels of glucose. (F) Protein levels of GLUT1, PKM2 and HK2 were quantified using western blotting. **P<0.01, ***P<0.001 vs. si-NC. Statistical significance was determined using one-way ANOVA followed by Tukey's post hoc test. ENO2, enolase 2; si-NC, small-interfering RNA negative control; ccRCC, clear cell renal cell carcinoma; ECAR, extracellular acidification rate; GLUT1, glucose transporter 1; PKM2, pyruvate kinase muscle isozyme M2; HK2, hexokinase 2.

Interference with ENO2 inhibits glycolysis levels in ccRCC cells. Additionally, to further study the mechanism of ENO2, transfection was used to interfere with the expression of ENO2 (Fig. 2A and B). Subsequently, the effect of ENO2 interference on glycolysis in ccRCC cell lines was studied. The levels of ECAR, lactic acid and glucose in Caki-1 cells were significantly reduced compared with those in the si-NC group (Fig. 2C-E). Moreover, western blotting showed that the protein expression of GLUT1, HK2 and PKM2 was decreased in the si-ENO2 Caki-1 cell group (Fig. 2F).

ENO2 interference promotes ferroptosis levels in ccRCC cells. The cytotoxicity of ferroptosis is associated with the production of ROS (22). To investigate the role of ROS in the si-ENO2-induced ferroptosis, the DCFH-DA probe was used to monitor intracellular ROS production. After ENO2 interference, total iron levels, intracellular ROS levels, MDA and 4-HNE levels were significantly increased, while the levels of SOD, GSH-Px and those of the ferroptosis-related proteins GPX4, FTH1 and SLC7A11 were significantly decreased; the protein expression of ACSL4 was significantly increased in Caki-1 cells (Fig. 3A-G). These results suggested that si-ENO2 induced ferroptosis in Caki-1 cells.

ENO2 interference affects mitochondrial function in ccRCC cells. Excessive ROS production changes the shape of mitochondria, leading to apoptosis. Moreover, mitochondrial membrane potential manifests normal structure and function of mitochondria, while depolarization of membrane potential indicates impaired mitochondrial structure and function (23,24). Hence, in the present study, a JC-1 fluorescence probe was used to measure mitochondrial membrane potential in ccRCC cells. Compared with the si-NC group, si-ENO2 significantly caused the depolarization of mitochondrial membrane potential in ccRCC cells (Fig. 4A). Furthermore, the mitochondrial ROS

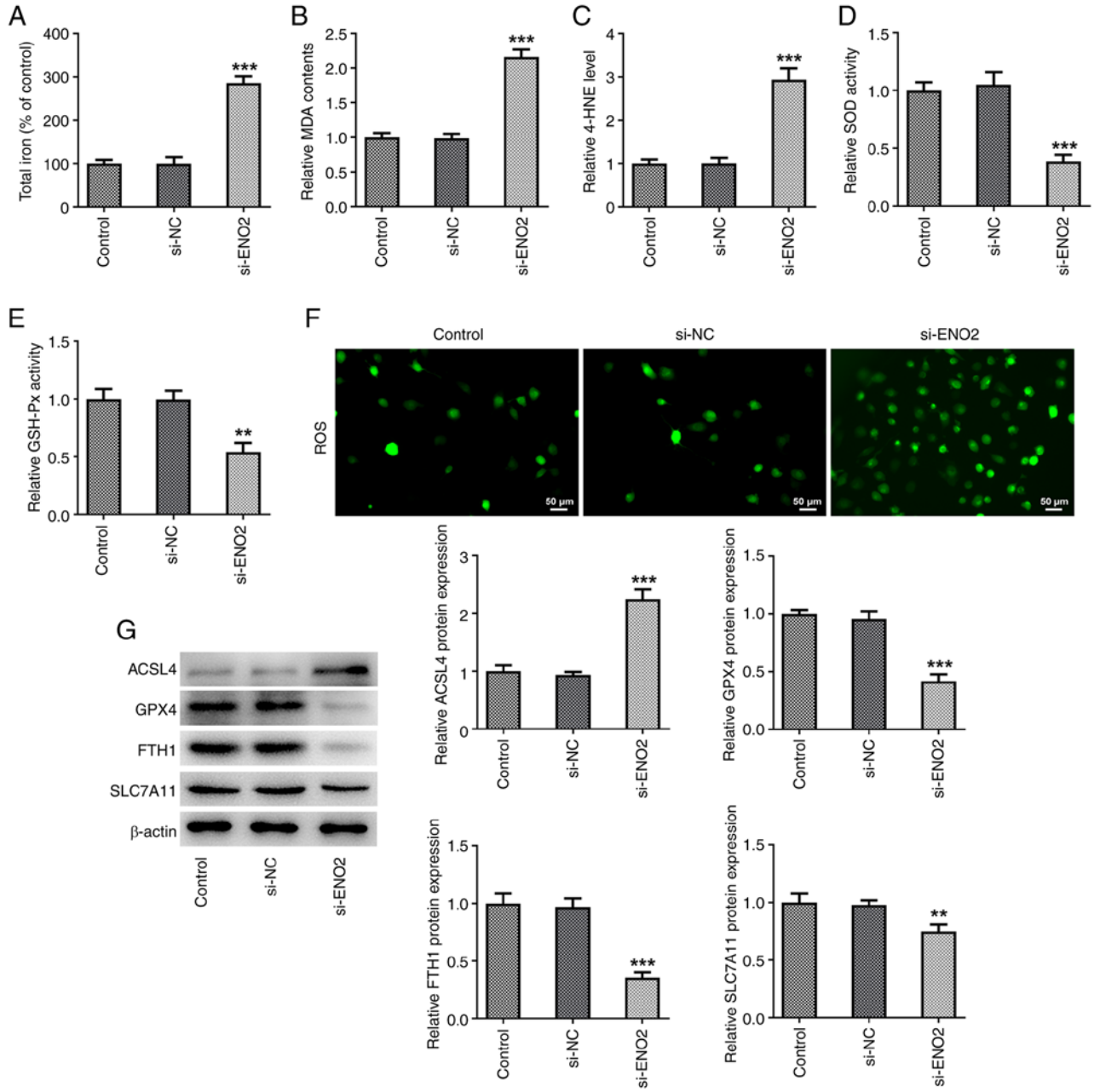

Figure 3. Effects of ENO2 interference on ferroptosis in clear cell renal cell carcinoma cells. (A) Total iron levels. (B) MDA level. (C) 4-HNE level. (D) SOD activity. (E) GSH-Px activity. (F) Intracellular reactive oxygen species levels. (G) Protein levels of ACSL4, GPX4, FTH1 and SLC7A11 estimated through western blotting. **P<0.01 and ***P<0.001 vs. si-NC. Statistical significance was determined using one-way ANOVA followed by Tukey's post hoc test. si-NC, small-interfering RNA negative control; MDA, malonaldehyde; 4-HNE, 4-hydroxynonenal; SOD, superoxide dismutase; GSH-Px, glutathione peroxidase; ACSL4, ferroptosis-related proteins acyl-CoA synthetase long-chain family member 4; GPX4, glutathione peroxidase 4; FTH1, ferritin heavy chain 1; SLC7A11, solute carrier family 7 member 11; ENO2, enolase 2.

content and membrane mPTP opening of ccRCC cells were increased, while the ATP content and mitochondrial oxidative phosphorylation capacity were decreased in ccRCC cells after interference with ENO2 (Fig. 4B-E).

ENO2 interference affects ferroptosis levels in ccRCC by inhibiting the glycolysis process. The aforementioned results showed that ENO2 had the highest impact on PKM2, so it was hypothesized that ENO2 may affect the glycolysis process through PKM2. Therefore, the PKM2 activator DASA-58 was used to treat ccRCC cells. To further explore whether ENO2 affects the level of ferroptosis in ccRCC cells by inhibiting the glycolytic process, the DCFH-DA probe was used to monitor intracellular ROS production. The results showed that adding the glycolysis agonist DASA-58 reversed the effects of interference with ENO2 on total iron levels and intracellular ROS, MDA and 4-HNE levels, SOD and GSH-Px activities, as well as expression of the ferroptosis-related proteins GPX4, FTH1, SLC7A11 and ACSL4 (Fig. 5A-G). These results indicated that si-ENO2 affects the level of ferroptosis in ccRCC cells by inhibiting the glycolytic process.

ENO2 interference affects ferroptosis and glycolysis by regulating Hippo-YAP1 signaling in ccRCC cells. To explore whether ENO2 affects ferroptosis and glycolysis by regulating

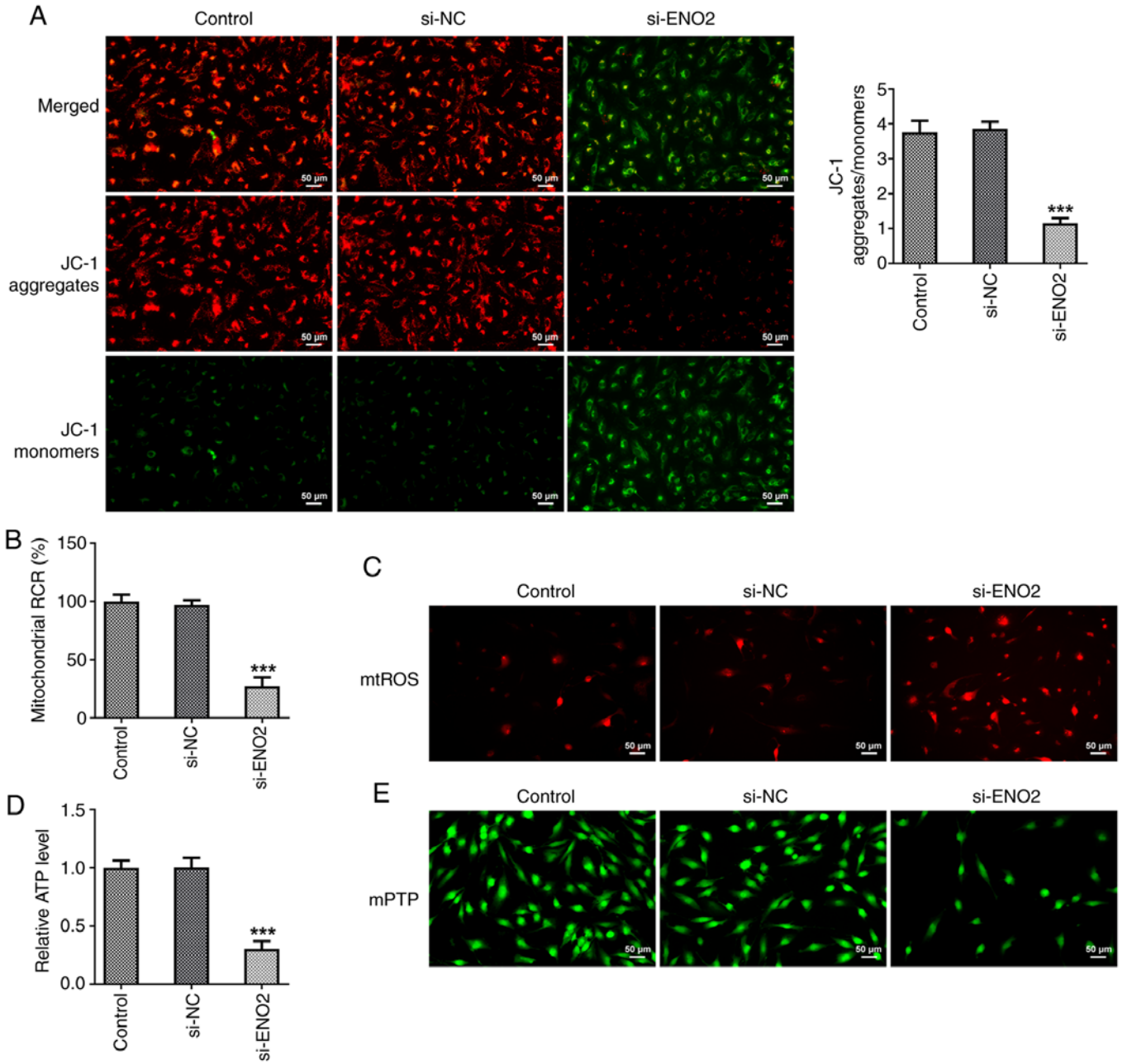

Figure 4. Effects of ENO2 interference on mitochondrial function in clear cell renal cell carcinoma cells. (A) Mitochondrial membrane potential was detected by using a JC-1 fluorescence probe. (B) Mitochondrial oxidative phosphorylation activity. (C) mtROS content. (D) ATP content. (E) Opening of mitochondrial membrane mPTP. ***P<0.001 vs. si-NC. Statistical significance was determined using one-way ANOVA followed by Tukey's post hoc test. si-NC, small-interfering RNA negative control; RCR: respiratory control ratios; mtROS, mitochondrial reactive oxygen species; mPTP, mitochondrial permeability transition pore; ENO2, enolase 2.

Hippo-YAP1 signaling in ccRCC cells, the expression levels of proteins related to the Hippo-YAP1 signaling pathway were investigated using western blotting. The results showed that after interference with ENO2, the expression of LATS1 and YAP1 were significantly downregulated in ccRCC cells (Fig. 6A). Subsequently, to further explore the effect of ENO2 on autophagy in ccRCC cells through the Hippo-YAP1 signaling, an overexpression plasmid of YAP1 was constructed, and western blotting was used to detect the expression level of YAP1 (Fig. 6B). The results indicated that YAP1 overexpression reversed the effects of ENO2 interference on total iron levels, intracellular ROS, MDA and 4-HNE levels, SOD and GSH-Px activities, as well as the expression of ferroptosis-related proteins GPX4, FTH1, SLC7A11 and ACSL4 proteins (Fig. 6C-F). These results suggest that si-ENO2 affects ferroptosis in ccRCC cells by regulating Hippo-YAP1 signaling. Subsequently, the effect of si-ENO2 + OV-YAP1 on glycolysis in ccRCC cells was studied. Compared with the si-ENO2 group, the si-ENO2 + OV-YAP1 group significantly increased ECAR, lactic acid and glucose levels in the culture medium by affecting Hippo-YAP1 signaling in ccRCC cells (Fig. 7A-C). Western blotting results also showed that the expression of GLUT1, HK2 and PKM2 were significantly increased in the si-ENO2 + OV-YAP1 group (Fig. 7D).

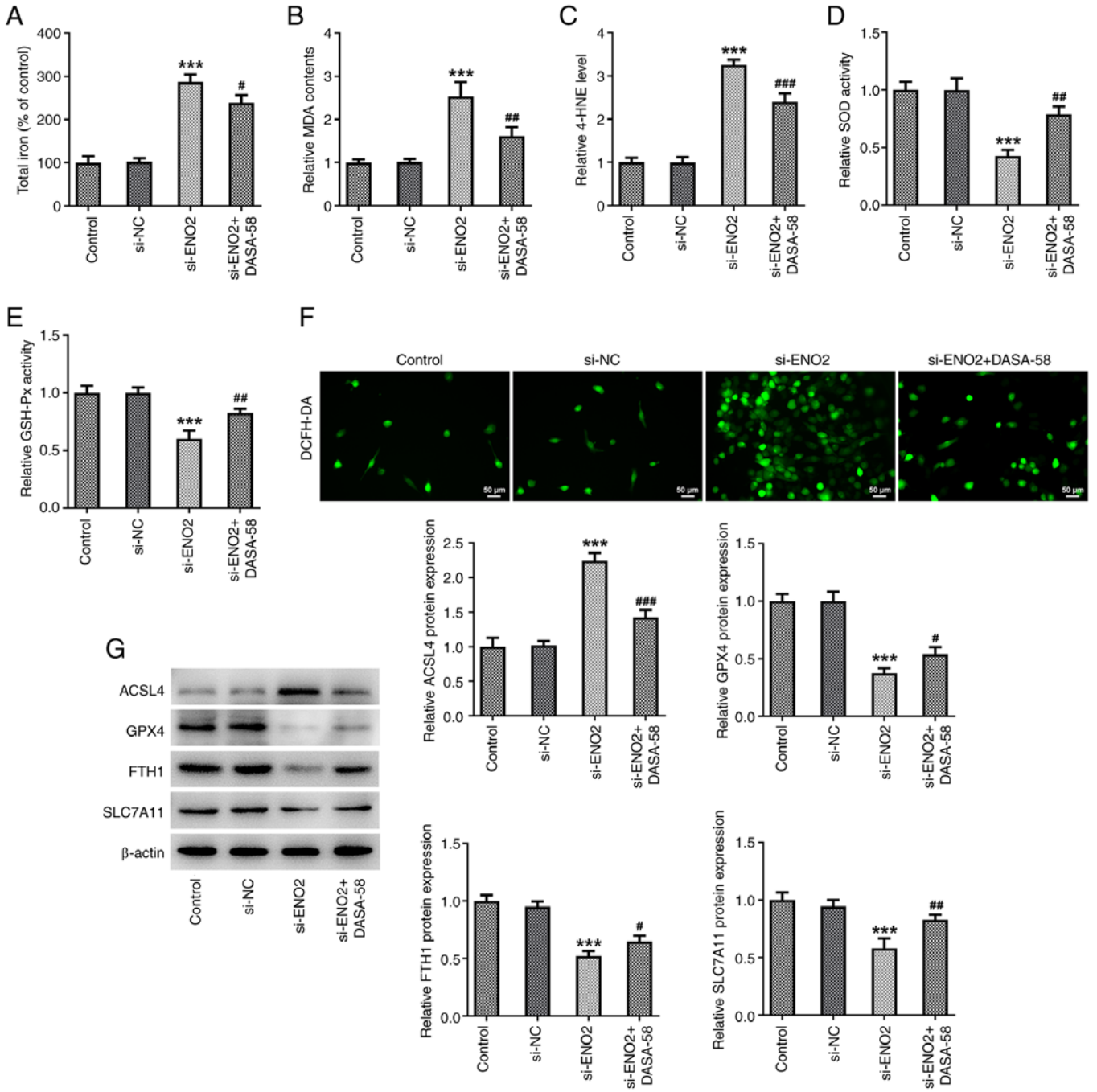

Figure 5. ENO2 interference affects ferroptosis levels in clear cell renal cell carcinoma cells by inhibiting the glycolysis process. (A) Total iron levels; (B) MDS level; (C) 4-HNE levels. (D) SOD activity; (E) GSH-Px activity. (F) Intracellular reactive oxygen species levels. (G) Protein levels of ACSL4, GPX4, FTH1 and SLC7A11 were estimated through western blotting. ***P<0.001 vs. si-NC, $^{\#}$P<0.05, $^{\#\#}$P<0.01, $^{\#\#\#}$P<0.001 vs. si-ENO2. Statistical significance was determined using one-way ANOVA followed by Tukey's post hoc test. si-NC, small-interfering RNA negative control; ENO2, enolase 2; si-ENO2, small-interfering RNA targeting ENO2; MDA, malonaldehyde; 4-HNE, 4-hydroxynonenal; SOD, superoxide dismutase; GSH-Px, glutathione peroxidase; ACSL4, ferroptosis-related proteins acyl-CoA synthetase long-chain family member 4; GPX4, glutathione peroxidase 4; FTH1, ferritin heavy chain 1; SLC7A11, solute carrier family 7 member 11.

Interference with ENO2 affects mitochondrial function by regulating Hippo-YAP1 signaling in ccRCC cells. The probe JC-1 is a sensitive fluorescent dye used to detect changes in mitochondrial membrane potential. Moreover, a change in JC-1 fluorescence emission from red to green indicates depolarization of the mitochondrial membrane. Further experiments in the present study showed that compared with interference with ENO2, the depolarization of the mitochondrial membrane potential in the si-ENO2+OV-YAP1 group was significantly improved (Fig. 8A). In addition, compared with interference with ENO2, the mitochondrial ROS content and membrane mPTP opening of ccRCC cells in the si-ENO2+OV-YAP1 group were reduced, while the ATP content and mitochondrial oxidative phosphorylation capacity were increased (Fig. 8B-E). These results demonstrated that interference with ENO2 affected mitochondrial function by modulating Hippo-YAP1 signaling in ccRCC cells.

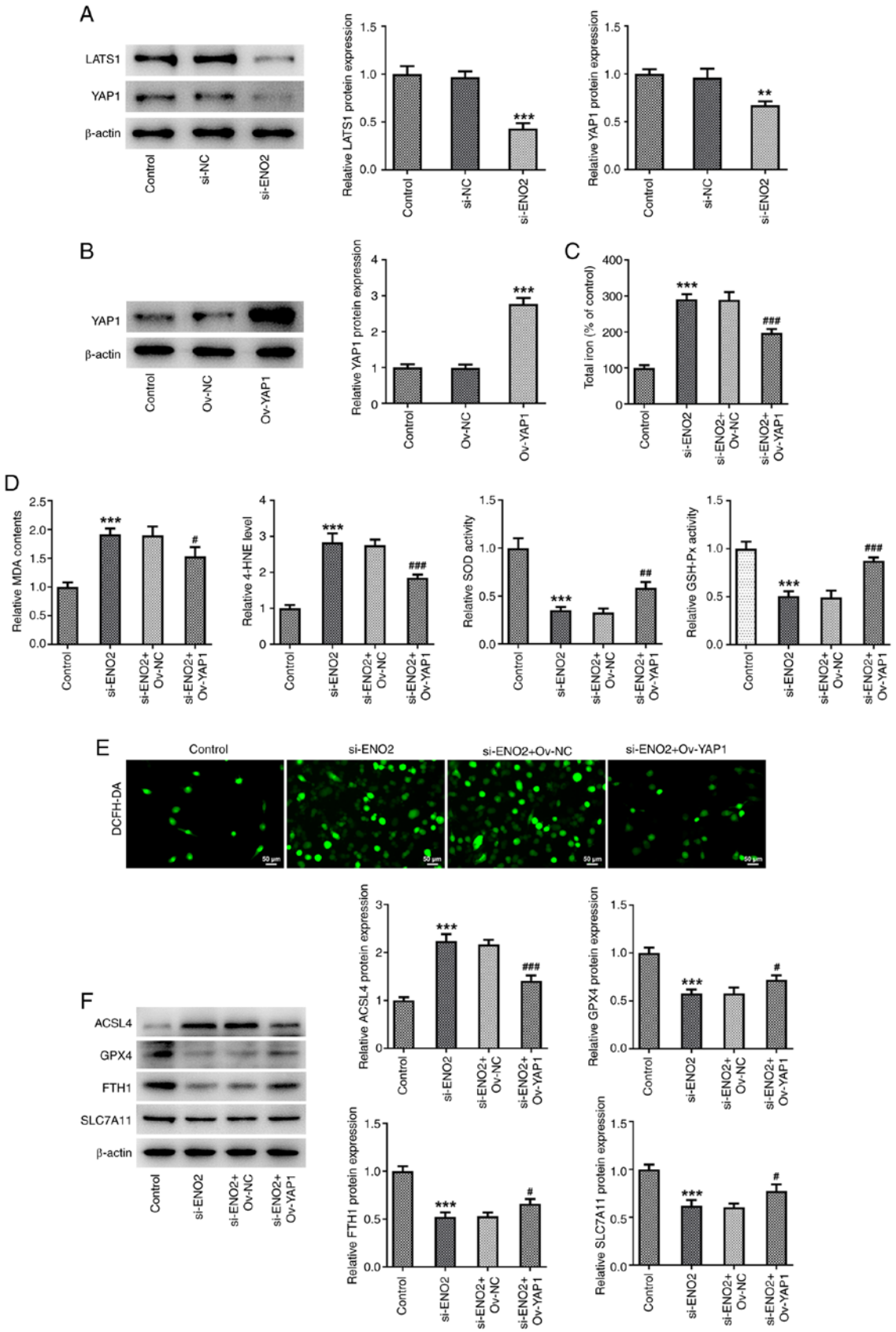

Figure 6. Effects of interference with ENO2 on ferroptosis through regulating Hippo-YAP1 signaling in ccRCC cells. (A) Protein levels of YAP1 and LATS1 were estimated by western blotting. (B) Protein levels of YAP1 were estimated by western blotting. (C) Total iron levels. (D) MDA, 4-HNE, SOD and GSH-Px levels. (E) Intracellular ROS levels. (F) Protein levels of ferroptosis-related proteins ACSL4, GPX4, FTH1 and SLC7A11 were estimated by western blotting. **P<0.01, ***P<0.001 vs. control, $^{\#}$P<0.05, $^{\#\#}$P<0.01, $^{\#\#\#}$P<0.001 vs. si-ENO2+Ov-YAP1. Statistical significance was determined using one-way ANOVA followed by Tukey's post hoc test. si-NC, small-interfering RNA negative control; ENO2, enolase 2; si-ENO2, small-interfering RNA targeting ENO2; ccRCC, clear cell renal cell carcinoma; MDA, malonaldehyde; 4-HNE, 4-hydroxynonenal; SOD, superoxide dismutase; GSH-Px, glutathione peroxidase; ACSL4, ferroptosis-related proteins acyl-CoA synthetase long-chain family member 4; GPX4, glutathione peroxidase 4; FTH1, ferritin heavy chain 1; SLC7A11, solute carrier family 7 member 11; ROS, reactive oxygen species; YAP1, yes-associated protein 1; LATS1, large tumor suppressor kinase 1; Ov, overexpression.

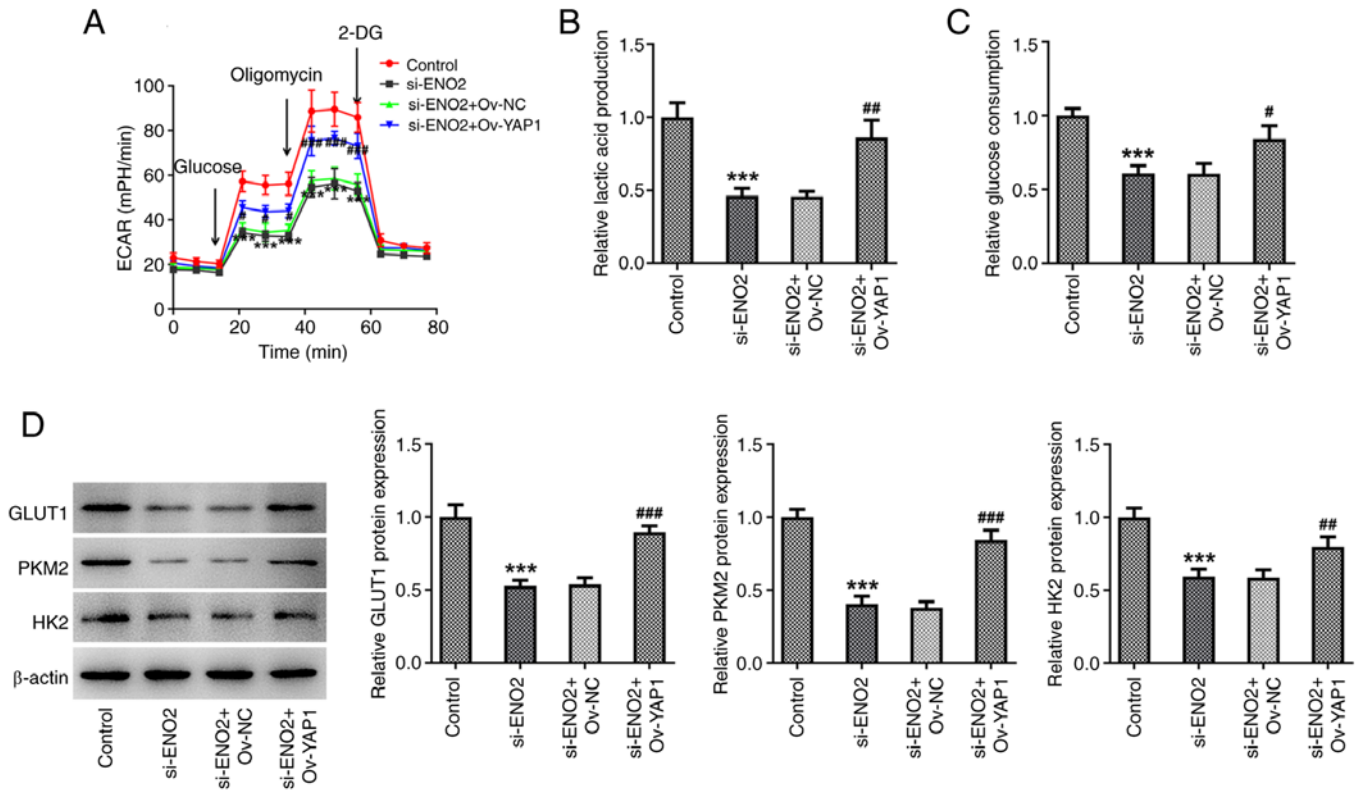

Figure 7. Effects of interference with ENO2 on glycolysis through regulating Hippo-YAP1 signaling in ccRCC cells. (A) ECAR assessment. (B) Levels of lactic acid. (C) Levels of glucose. (D) Protein levels of GLUT1, PKM2 and HK2 estimated by western blotting. ***P<0.001 vs. control, $^{\#}$P<0.05, $^{\#\#}$P<0.01, $^{\#\#\#}$P<0.001 vs. si-ENO2+Ov-YAP1. Statistical significance was determined using one-way ANOVA followed by Tukey's post hoc test. si-NC, small-interfering RNA negative control; ENO2, enolase 2; si-ENO2, small-interfering RNA targeting ENO2; YAP1, yes-associated protein 1; ccRCC, clear cell renal cell carcinoma; ECAR, extracellular acidification rate; GLUT1, glucose transporter 1; PKM2, pyruvate kinase muscle isozyme M2; HK2, hexokinase 2; Ov, overexpression.

Discussion

Tumor cells manifest aberrant metabolism characterized by excessive glycolysis even in the presence of sufficient amounts of oxygen. This phenomenon, also known as aerobic glycolysis or Warburg effect, promotes cancer growth with accelerated glucose uptake and lactic acid production (25,26). Glycolysis is quite crucial in cancer, and cancer cells exhibit elevated expression of key enzymes (including GLUT1, PKM2 and HK2) involved in the process of glycolysis to lead to increased amounts of energy. Furthermore, cancer cells can produce energy via fermentation of lactic acid, a product of glycolysis (27). Glycolytic genes and the Warburg effect have been studied in bladder, breast, gastric, liver and prostate cancer (28-31). Previous research demonstrated that the Warburg effect is more noticeable in ccRCC than in other tumors (32). Metabolic profiling-based studies showed that ccRCC manifests as increased metabolite levels during glycolysis and decreased metabolite levels during oxidative phosphorylation, indicating that glycolysis is active in ccRCC (33-35). Hence, the present study investigated the expression of glycolysis-related genes in ccRCC cell lines to identify biomarkers that can predict disease prognosis.

ENO2 is a critical gene in glycolysis that can stimulate cell growth, upregulate glycolysis-related genes and initiate the Akt signaling pathway by phosphorylation of glycogen synthase kinase 3β, thereby inducing cell proliferation and glycolysis (14). Increased ENO2 expression is found in various tumors. High expression of ENO2 in glioma and colorectal cancer is linked to glycolysis in tumor cells (36,37). Increased ENO2 expression stimulates glycolysis in gastric cancer cells, contributing to tumor growth and liver metastasis (38). Regarding the Warburg effect in ccRCC, previous research proposed that ENO2 expression is notably increased in tissue and serum of patients with ccRCC (39,40). Additionally, elevated serum ENO2 levels are associated with clinical stage, tumor grade and disease recurrence. Thus, ENO2 is a potential biomarker for ccRCC prognosis (41,42). The present data showed that ENO2 expression was more prominent in ccRCC cell lines compared with that in HK-2 normal human renal tubular epithelial cell lines. Furthermore, the levels of ECAR, lactic acid and glucose in the Caki-1 cells culture medium were significantly reduced. Moreover, western blotting showed that the expression of GLUT1, HK2 and PKM2 was decreased in the si-ENO2 Caki-1 cells group. Thus, ENO2 served a critical function in inhibiting glycolysis of ccRCC cells, which is consistent with previous research (37).

Previous studies reported that ferroptosis exerts a crucial role in ischemic organ damage, neurodegenerative diseases and tumor cell death (43,44). Furthermore, recent research suggested that ferroptosis is considered a targeted susceptibility and exerts tumor suppressor effects by killing tumor cells in ccRCC (45,46). Thus, triggering ferroptosis could be a novel promising strategy for treating cancers. The present study also revealed that total iron levels, intracellular ROS, MDA and 4-HNE levels, and the protein expression of ACSL4 were significantly increased, while SOD and GSH-Px

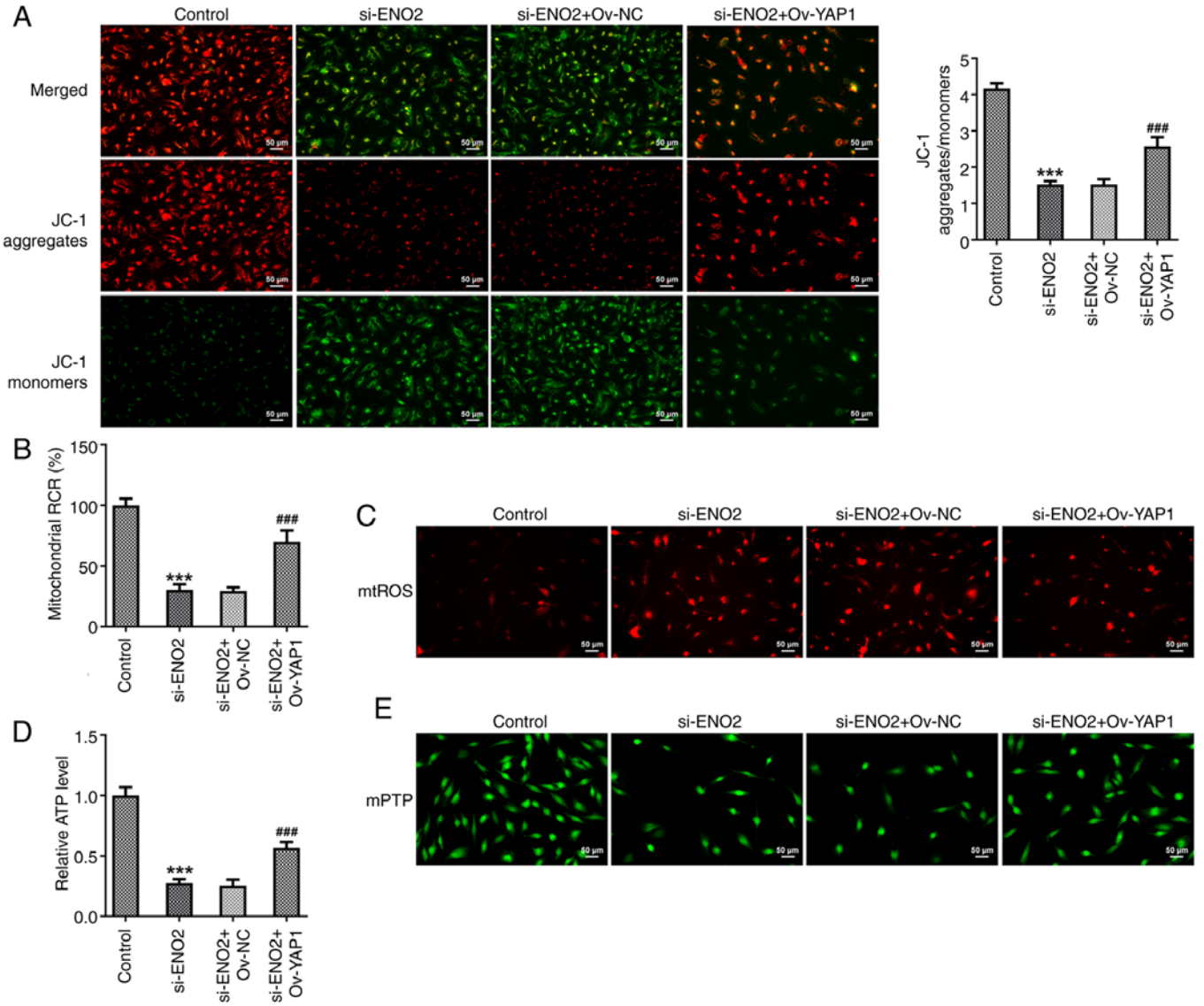

Figure 8. Effects of interference with ENO2 on mitochondrial function through regulating Hippo-YAP1 signaling in ccRCC cells. (A) Mitochondrial membrane potential was detected using a JC-1 fluorescence probe. (B) Capacity of mitochondrial oxidative phosphorylation. (C) mtROS content. (D) ATP content. (E) The opening of mitochondrial membrane mPTP. ***P<0.001 vs. control, $^{###}$P<0.001 vs. si-ENO2+Ov-YAP1. Statistical significance was determined using one-way ANOVA followed by Tukey's post hoc test. si-NC, small-interfering RNA negative control; ENO2, enolase 2; si-ENO2, small-interfering RNA targeting ENO2; YAP1, yes-associated protein 1; ccRCC, clear cell renal cell carcinoma; Ov, overexpression; mtROS, mitochondrial reactive oxygen species; mPTP, mitochondrial permeability transition pore; RCR, respiratory control ratio.

activities and the protein expression of GPX4, FTH1 and SLC7A11 were significantly decreased after interference with ENO2 in ccRCC cells. These results suggested that ENO2 interference induced ferroptosis in ccRCC cells. Moreover, iron overload causes cardiac mitochondrial dysfunction as indicated by increased mitochondrial ROS levels and mitochondrial membrane potential depolarization (47). Additionally, mitochondria are essential organelles in cells and closely linked to ferroptosis in recent studies (48,49). The present study suggested that the interference of ENO2 caused the depolarization of mitochondrial membrane potential, increased mitochondrial ROS content, decreased ATP content and induced ROS accumulation, thereby disrupting mitochondrial function in ccRCC cells. Since the current study showed that ENO2 has the greatest impact on PKM2, it was further explored whether ENO2 affects glycolysis through PKM2, thereby affecting the level of ferroptosis in ccRCC cells. DASA-58, a highly specific small-molecule PKM2 activator, leads to a decrease in glycolytic and pentose phosphate pathway intermediates by activating the enzyme (50). Furthermore, PKM2 is directly involved in the metabolic reprogramming (aerobic glycolysis) associated with cancer and the inflammatory response (51-53). The present results indicated that ENO2 interference affected the level of ferroptosis in ccRCC cells by inhibiting the glycolytic process. A recent study demonstrated that ENO2 inhibited the activation of the Hippo-YAP1 pathway, thereby inducing ferroptosis in small-cell lung cancer cells (20). It was shown that interference of ENO2 could modulate Hippo-YAP1 signaling in ccRCC cells. In addition, interference of ENO2 affects ferroptosis, glycolysis and mitochondrial function by regulating Hippo-YAP1 signaling in ccRCC cells.

The current study has a certain limitation that should be acknowledged; it lacks further validation of the use of ferroptosis inhibitors when conducting ferroptosis studies. Therefore, it is crucial to use ferroptosis to further verify the in-depth mechanisms of ENO2 interference affecting ferroptosis levels in ccRCC.

Collectively, the present study demonstrates that ENO2 is expressed at high levels in ccRCC cells, and interference of ENO2 inhibits glycolysis, promotes ferroptosis levels and affects mitochondrial function by regulating Hippo-YAP1 signaling in ccRCC cells.

Acknowledgements

Not applicable.

Funding

No funding was received.

Availability of data and materials

The data generated in the present study may be requested from the corresponding author.

Authors' contributions

HL and XL conceived and designed the study. YW acquired and interpreted the data. HL was a major contributor in writing the manuscript. YM collected and analyzed the data. HL, XL and YM confirm the authenticity of all the raw data. All authors read and approved the final version of the manuscript.

Ethics approval and consent to participate

Not applicable.

Patient consent for publication

Not applicable.

Competing interests

The authors declare that they have no competing interests.

References

1. Bray F, Ferlay J, Soerjomataram I, Siegel RL, Torre LA and Jemal A: Global cancer statistics 2018: GLOBOCAN estimates of incidence and mortality worldwide for 36 cancers in 185 countries. CA Cancer J Clin 68: 394-424, 2018.
2. Motzer RJ, Bacik J and Mazumdar M: Prognostic factors for survival of patients with stage IV renal cell carcinoma: Memorial sloan-kettering cancer center experience. Clin Cancer Res 10: 6302S-6303S, 2004.
3. Jonasch E, Gao J and Rathmell WK: Renal cell carcinoma. BMJ 349: g4797, 2014.
4. Pavlova NN and Thompson CB: The emerging hallmarks of cancer metabolism. Cell Metab 23: 27-47, 2016.
5. Miranda-Galvis M and Teng Y: Targeting Hypoxia-driven metabolic reprogramming to constrain tumor progression and metastasis. Int J Mol Sci 21: 5487, 2020.
6. Zhang Y, Chen M, Liu M, Xu Y and Wu G: Glycolysis-related genes serve as potential prognostic biomarkers in clear cell renal cell carcinoma. Oxid Med Cell Longev 2021: 6699808, 2021.
7. Tang B, Yan R, Zhu J, Cheng S, Kong C, Chen W, Fang S, Wang Y, Yang Y, Qiu R, *et al*: Integrative analysis of the molecular mechanisms, immunological features and immunotherapy response of ferroptosis regulators across 33 cancer types. Int J Biol Sci 18: 180-198, 2022.
8. Torti SV and Torti FM: Iron and cancer: 2020 Vision. Cancer Res 80: 5435-5448, 2020.
9. Dixon SJ, Lemberg KM, Lamprecht MR, Skouta R, Zaitsev EM, Gleason CE, Patel DN, Bauer AJ, Cantley AM, Yang WS, *et al*: Ferroptosis: An iron-dependent form of nonapoptotic cell death. Cell 149: 1060-1072, 2012.
10. Hao J, Chen Q, Feng Y, Jiang Q, Sun H, Deng B, Huang X, Guan J, Chen Q, Liu X, *et al*: Combination treatment with FAAH inhibitors/URB597 and ferroptosis inducers significantly decreases the growth and metastasis of renal cell carcinoma cells via the PI3K-AKT signaling pathway. Cell Death Dis 14: 247, 2023.
11. Reed GH, Poyner RR, Larsen TM, Wedekind JE and Rayment I: Structural and mechanistic studies of enolase. Curr Opin Struct Biol 6: 736-743, 1996.
12. Zheng Y, Wu C, Yang J, Zhao Y, Jia H, Xue M, Xu D, Yang F, Fu D, Wang C, *et al*: Insulin-like growth factor 1-induced enolase 2 deacetylation by HDAC3 promotes metastasis of pancreatic cancer. Signal Transduct Target Ther 5: 53, 2020.
13. Marangos PJ, Parma AM and Goodwin FK: Functional properties of neuronal and glial isoenzymes of brain enolase. J Neurochem 31: 727-732, 1978.
14. Liu CC, Wang H, Wang WD, Wang L, Liu WJ, Wang JH, Geng QR and Lu Y: ENO2 promotes cell proliferation, glycolysis, and glucocorticoid-resistance in acute lymphoblastic leukemia. Cell Physiol Biochem 46: 1525-1535, 2018.
15. Huebbers CU, Adam AC, Preuss SF, Schiffer T, Schilder S, Guntinas-Lichius O, Schmidt M, Klussmann JP and Wiesner RJ: High glucose uptake unexpectedly is accompanied by high levels of the mitochondrial ß-F1-ATPase subunit in head and neck squamous cell carcinoma. Oncotarget 6: 36172-36184, 2015.
16. Huang J, Yang M, Liu Z, Li X, Wang J, Fu N, Cao T and Yang X: PPFIA4 promotes colon cancer cell proliferation and migration by enhancing tumor glycolysis. Front Oncol 11: 653200, 2021.
17. Liu C, Liu D, Wang F, Xie J, Liu Y, Wang H, Rong J, Xie J, Wang J, Zeng R, *et al*: Identification of a glycolysis- and lactate-related gene signature for predicting prognosis, immune microenvironment, and drug candidates in colon adenocarcinoma. Front Cell Dev Biol 10: 971992, 2022.
18. Lang L, Wang F, Ding Z, Zhao X, Loveless R, Xie J, Shay C, Qiu P, Ke Y, Saba NF and Teng Y: Blockade of glutamine-dependent cell survival augments antitumor efficacy of CPI-613 in head and neck cancer. J Exp Clin Cancer Res 40: 393, 2021.
19. Lv C, Yu H, Wang K, Chen C, Tang J, Han F, Mai M, Ye K, Lai M and Zhang H: ENO2 promotes colorectal cancer metastasis by interacting with the LncRNA CYTOR and activating YAP1-induced EMT. Cells 11: 2363, 2022.
20. Zheng S, Mo J, Zhang J and Chen Y: HIF-1α inhibits ferroptosis and promotes malignant progression in non-small cell lung cancer by activating the Hippo-YAP signalling pathway. Oncol Lett 25: 90, 2023.
21. Liu G, Zhou J, Piao Y, Zhao X, Zuo Y and Ji Z: Hsa_circ_0085576 promotes clear cell renal cell carcinoma tumorigenesis and metastasis through the miR-498/YAP1 axis. Aging (Albany NY) 12: 11530-11549, 2020.
22. Wang J, Zhao Z, Liu Y, Cao X, Li F, Ran H, Cao Y and Wu C: 'Mito-Bomb': A novel mitochondria-targeting nanosystem for ferroptosis-boosted sonodynamic antitumor therapy. Drug Deliv 29: 3111-3122, 2022.
23. Zhang M, Zhong H, Cao T, Huang Y, Ji X, Fan GC and Peng T: Gamma-aminobutyrate transaminase protects against lipid overload-triggered cardiac injury in mice. Int J Mol Sci 23: 2182, 2022.
24. Huang SX, Partridge MA, Ghandhi SA, Davidson MM, Amundson SA and Hei TK: Mitochondria-derived reactive intermediate species mediate asbestos-induced genotoxicity and oxidative stress-responsive signaling pathways. Environ Health Perspect 120: 840-847, 2012.
25. Doherty JR and Cleveland JL: Targeting lactate metabolism for cancer therapeutics. J Clin Invest 123: 3685-3692, 2013.
26. Liberti MV and Locasale JW: The Warburg effect: How does it benefit cancer cells? Trends Biochem Sci 41: 211-218, 2016.
27. Abbaszadeh Z, Çeşmeli S and Biray Avcı Ç: Crucial players in glycolysis: Cancer progress. Gene 726: 144158, 2020.

28. Guo Y, Liang F, Zhao F and Zhao J: Resibufogenin suppresses tumor growth and Warburg effect through regulating miR-143-3p/HK2 axis in breast cancer. Mol Cell Biochem 466: 103-115, 2020.
29. Han S, Yang S, Cai Z, Pan D, Li Z, Huang Z, Zhang P, Zhu H, Lei L and Wang W: Anti-Warburg effect of rosmarinic acid via miR-155 in gastric cancer cells. Drug Des Devel Ther 9: 2695-2703, 2015.
30. Zheng J, Luo J, Zeng H, Guo L and Shao G: ^{125}I suppressed the Warburg effect viaregulating miR-338/PFKL axis in hepatocellular carcinoma. Biomed Pharmacother 119: 109402, 2019.
31. Liu Y, Liang T, Qiu X, Ye X, Li Z, Tian B and Yan D: Down-regulation of Nfatc1 suppresses proliferation, migration, invasion, and Warburg effect in prostate cancer cells. Med Sci Monit 25: 1572-1581, 2019.
32. Morais M, Dias F, Teixeira AL and Medeiros R: MicroRNAs and altered metabolism of clear cell renal cell carcinoma: Potential role as aerobic glycolysis biomarkers. Biochim Biophys Acta Gen Subj 1861: 2175-2185, 2017.
33. Hakimi AA, Reznik E, Lee CH, Creighton CJ, Brannon AR, Luna A, Aksoy BA, Liu EM, Shen R, Lee W, *et al*: An integrated metabolic atlas of clear cell renal cell carcinoma. Cancer Cell 29: 104-116, 2016.
34. Grønningsæter IS, Fredly HK, Gjertsen BT, Hatfield KJ and Bruserud O: Systemic metabolomic profiling of acute myeloid leukemia patients before and during disease-stabilizing treatment based on all-trans retinoic acid, valproic acid, and low-dose chemotherapy. Cells 8: 1229, 2019.
35. Fang Z, Sun Q, Yang H and Zheng J: SDHB suppresses the tumorigenesis and development of ccRCC by inhibiting glycolysis. Front Oncol 11: 639408, 2021.
36. Kounelakis MG, Zervakis ME, Giakos GC, Postma GJ, Buydens LM and Kotsiakis X: On the relevance of glycolysis process on brain gliomas. IEEE J Biomed Health Inform 17: 128-135, 2013.
37. Yeh CS, Wang JY, Chung FY, Lee SC, Huang MY, Kuo CW, Yang MJ and Lin SR: Significance of the glycolytic pathway and glycolysis related-genes in tumorigenesis of human colorectal cancers. Oncol Rep 19: 81-91, 2008.
38. Wang Q, Chen C, Ding Q, Zhao Y, Wang Z, Chen J, Jiang Z, Zhang Y, Xu G, Zhang J, *et al*: METTL3-mediated m^{6}A modification of HDGF mRNA promotes gastric cancer progression and has prognostic significance. Gut 69: 1193-1205, 2020.
39. Sanders E and Diehl S: Analysis and interpretation of transcriptomic data obtained from extended Warburg effect genes in patients with clear cell renal cell carcinoma. Oncoscience 2: 151-186, 2015.
40. Teng PN, Hood BL, Sun M, Dhir R and Conrads TP: Differential proteomic analysis of renal cell carcinoma tissue interstitial fluid. J Proteome Res 10: 1333-1342, 2011.
41. Rasmuson T, Grankvist K and Ljungberg B: Serum gamma-enolase and prognosis of patients with renal cell carcinoma. Cancer 72: 1324-1328, 1993.
42. Takashi M, Sakata T and Kato K: Use of serum gamma-enolase and aldolase A in combination as markers for renal cell carcinoma. Jpn J Cancer Res 84: 304-309, 1993.
43. Qiu Y, Cao Y, Cao W, Jia Y and Lu N: The application of ferroptosis in diseases. Pharmacol Res 159: 104919, 2020.
44. Li Y, Feng D, Wang Z, Zhao Y, Sun R, Tian D, Liu D, Zhang F, Ning S, Yao J and Tian X: Ischemia-induced ACSL4 activation contributes to ferroptosis-mediated tissue injury in intestinal ischemia/reperfusion. Cell Death Differ 26: 2284-2299, 2019.
45. Zou Y, Henry WS, Ricq EL, Graham ET, Phadnis VV, Maretich P, Paradkar S, Boehnke N, Deik AA, Reinhardt F, *et al*: Plasticity of ether lipids promotes ferroptosis susceptibility and evasion. Nature 585: 603-608, 2020.
46. Wang J, Yin X, He W, Xue W, Zhang J and Huang Y: SUV39H1 deficiency suppresses clear cell renal cell carcinoma growth by inducing ferroptosis. Acta Pharm Sin B 11: 406-419, 2021.
47. Kumfu S, Chattipakorn S, Fucharoen S and Chattipakorn N: Mitochondrial calcium uniporter blocker prevents cardiac mitochondrial dysfunction induced by iron overload in thalassemic mice. Biometals 25: 1167-1175, 2012.
48. Fang X, Wang H, Han D, Xie E, Yang X, Wei J, Gu S, Gao F, Zhu N, Yin X, *et al*: Ferroptosis as a target for protection against cardiomyopathy. Proc Natl Acad Sci USA 116: 2672-2680, 2019.
49. She H, Tan L, Du Y, Zhou Y, Guo N, Zhang J, Du Y, Wang Y, Wu Z, Ma C, *et al*: VDAC2 malonylation participates in sepsis-induced myocardial dysfunction via mitochondrial-related ferroptosis. Int J Biol Sci 19: 3143-3158, 2023.
50. Anastasiou D, Yu Y, Israelsen WJ, Jiang JK, Boxer MB, Hong BS, Tempel W, Dimov S, Shen M, Jha A, *et al*: Pyruvate kinase M2 activators promote tetramer formation and suppress tumorigenesis. Nat Chem Biol 8: 839-847, 2012.
51. Yang L, Xie M, Yang M, Yu Y, Zhu S, Hou W, Kang R, Lotze MT, Billiar TR, Wang H, *et al*: PKM2 regulates the Warburg effect and promotes HMGB1 release in sepsis. Nat Commun 5: 4436, 2014.
52. Rao J, Wang H, Ni M, Wang Z, Wang Z, Wei S, Liu M, Wang P, Qiu J, Zhang L, *et al*: FSTL1 promotes liver fibrosis by reprogramming macrophage function through modulating the intracellular function of PKM2. Gut 71: 2539-2550, 2022.
53. Zhou X, Xie F, Wang L, Zhang L, Zhang S, Fang M and Zhou F: The function and clinical application of extracellular vesicles in innate immune regulation. Cell Mol Immunol 17: 323-334, 2020.